

A 3D Investigation of Geological Structure and Its Relationship to Mineralization in the Nanling-Xuancheng Ore District, Middle-Lower Yangtze River Metallogenic Belt, China


Sanming Lu^{1*}, Xueyi Lan², Lili Zhao¹, Zanzan Zhang¹, Xiaoyong Yang⁴, Zhuang Zhao⁴,
Dong Guo², Xiaochun Xu³, Yongsheng Wang³, Jianshe Li¹, Huasheng Qi⁴

1. Public Geological Survey Management Center of Anhui Province, Hefei 230091, China

2. Geological Exploration Technology Institute of Anhui Province, Hefei 230031, China

3. School of Resources and Environmental Engineering, Hefei University of Technology, Hefei 230009, China

4. CAS Center for Excellence in Comparative Planetology, University of Science and Technology of China, Hefei 230026, China

 Sanming Lu: <https://orcid.org/0000-0003-1093-9700>

ABSTRACT: The Nanling-Xuancheng ore region of Anhui Province is located in the Middle-Lower Yangtze River metallogenic belt. Insufficient exploration and research have been carried out in this newly defined ore district, although the Chating large porphyry Cu-Au deposit and a few middle-sized skarn-type Cu polymetallic deposits have been discovered. In this study, we carried out high-resolution seismic reflection, magnetotelluric, gravity, and magnetic investigations, and constructed the 3D geological structure of the uppermost crust in a depth range of 0–5 km using a comprehensive inversion of the new data constrained by previous deep-drilling data. We hence proposed some new insights to understand the mineralization processes of this district. A system of alternating ridges and valleys is suggested as the major structure pattern, composed of “two-layer structure” of the basins and “three-layer structure” of anticlines. Moreover, a conjugated fault system and its distribution features are revealed in our models, including the Jiangnan fault, Zhouwang fault, and Kunshan thrust nappe. The Jiangnan and Kunshan faults are suggested to have controlled the diagenesis and metallogenesis. Two deep concealed plutons located in Chating and Magushan are found, forming the Mesozoic diorite-felsic intrusions. These intrusions are believed to be the causes of hydrothermal deposits such as the Chating deposit and the Magushan deposit.

KEY WORDS: geophysical exploration, 3D structure, metallogenic mechanism, Nanling-Xuancheng ore region, Middle-Lower Yangtze River metallogenic belt, ore deposits.

0 INTRODUCTION

The Middle-Lower Yangtze River metallogenic belt (MLYB) is the most important Fe-Cu enrichment region of China (Fig. 1a; Lü et al., 2021). More than 200 ore deposits have been found in the seven districts, namely E’dongnan, Jiurui, Anqing-Guichi, Tongling, Luzong, Ningwu, and Ningzhen ore districts (Lü et al., 2020; Zhou et al., 2016). After some new Cu-Au polymetallic deposits (e.g., Chating porphyry Cu-Au deposit; Tongshan-Qiaomiashan, Magushan, and Shizishan skarn-type Cu-Mo-S-W deposits; Fig. 1b) were discovered in the Nanling-Xuancheng region by the recent geophysical and geologi-

cal explorations (Qian et al., 2017; Liu, 2016), this region can be defined as the eighth ore district in the MLYB (Fig. 1b).

The 3D structure exploration has been applied successfully in typical ore districts, such as that of North America and Australia (Heinson et al., 2018). Moreover, the 3D comprehensive geophysical exploration has been implemented in the MLYB at three levels, including regional lithospheric structure, 3D crustal structure of typical ore district, and structure of typical deposit in the most surface crust. In this project, high-resolution seismic reflection (Lü et al., 2015, 2014, 2013, 2012), magnetotelluric (MT) (Yan et al., 2019; Zhang et al., 2019, 2015; Tang et al., 2014, 2013; Xiao et al., 2014, 2011), and gravity and magnetic surveys (Lan et al., 2015; Guo et al., 2014; Qi et al., 2014; Yan et al., 2014, 2009) have been carried out in the Luzong, Ningwu and Tongling ore districts, revealing the 3D structure and the major ore-controlling factors. The study results could better the understanding of the deep structure, process and tectonic evolution for the ore district.

*Corresponding author: lusanming5101@sina.com

© China University of Geosciences (Wuhan) and Springer-Verlag GmbH Germany, Part of Springer Nature 2022

Manuscript received April 26, 2021.

Manuscript accepted November 16, 2021.

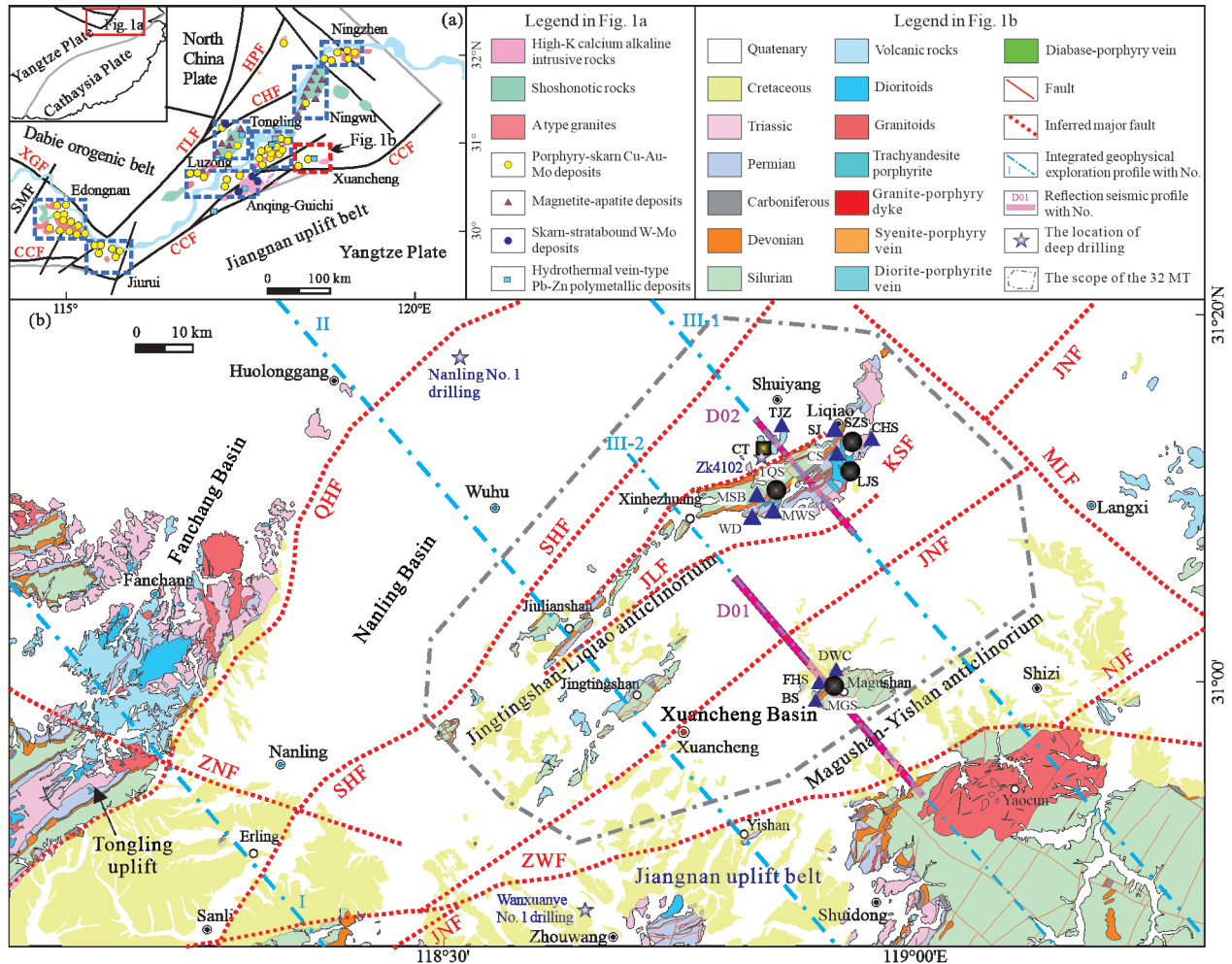


Figure 1. (a) Sketch geological map of magmatic rocks and deposits in the MLYB (modified after Lü et al., 2021; Zhou et al., 2017; Mao et al., 2011), (b) geological map of magmatic, deposits and projects arrangement in the NXOR. XGF. Xiangfan-Guangji fault; TLF. Tancheng-Lujiang fault; HPF. Huanglishu-Poliangting fault; SMF. Shangcheng-Magushan fault; CCF. Chongyang-Changzhou fault; CHF. Chuhe fault; QHF. Qingshui-Hewan fault; SHF. Sanlizhen-Hexizhen fault; LQF. Liqiao fault; KSF. Kunshan fault; JNF. Jiangnan fault; ZWF. Zhouwang fault; NJF. Ningguo-Jixi fault; ZNF. Zhongming-Nanling fault; MLF. Ma'anshan-Langxi fault. Porphyry deposit: CT. Chating Cu-Au deposit; skarn type deposits: SZS. Shizishan Cu-Mo deposit; LJS. Liujianshan S-Fe deposit; TQS. Tongshan-Qiaomaishan Cu-S(-W) deposit; MGS. Magushan Cu-Mo deposit; hydrothermal vein-type deposits: CHS. Changshan Pb-Zn deposit; SJ. Shuangjing Pb-Zn-Au-Ag deposit; CS. Chashan Pb-Zn ore spot; TJZ. Tangjiayui Pb-Zn ore spot; MSB. Mashanbu Pb-Zn ore spot; MWS. Maweishan Cu-S ore spot; WD. Weidun Pb-Zn ore spot; DWC. Dawangcun Pb-Zn ore spot; FHS. Fenghuangshan Pb-Zn ore spot; BS. Beishan Pb-Zn ore spot.

However, multi-discipline geophysical deep probes are insufficient in the new Nanling-Xuancheng district, though a series of geological and geochemical researches have been carried out for the deposits (e.g., Xu et al., 2020, 2018; Xiao et al., 2019, 2018; Feng et al., 2018; Ji, 2018; Wang, 2018; Xie et al., 2018; Hong et al., 2017; Jiang et al., 2017, 2015; Qian et al., 2017; Liu, 2016; Liu and Duan, 2015). Furthermore, due to the widespread Quaternary covers, the tectonic framework, magmatism and deposit genesis cannot be studied systematically using surface evidences, and the mineralization and related geodynamic processes have not been clearly understood.

To reveal the 3D geological structure of the study area, we carried out the comprehensive geophysical deep probes, including three profiles of geology, high-resolution seismic reflection, magnetotelluric (MT), gravity and magnet. In addition, another 32 MT profiles were arrayed covering the entire NXOR. Based on the geophysical results, we hence revealed the 3D

geological structure of this new ore district in a depth range of 0–5 000 m constrained by previous deep-drilling data, and discussed the genesis and relationship between structure and mineralization.

1 REGIONAL GEOLOGY

The MLYB is located in the Yangtze River fault depression region, which is the collisional foreland between the North China and Yangtze blocks in the Late Triassic (Fig. 1a; Zhou et al., 2017; Mao et al., 2011). Three major evolution stages have been occurred in the MLYB, including the development of Mesoproterozoic basement (Dongling Group) and Paleozoic covers, and intraplate deformation during the Mesozoic (Chang et al., 2019, 1991; Dong et al., 2011). Therefore, the present structural pattern of “uplift and depression” can be attributed to the multiple tectonic-magmatism since the Mesozoic (Zhou et al., 2008). The NXOR is a newly defined ore dis-

tract in the MLYB, composed of a Mesozoic–Cenozoic volcanic rift depression (Xu et al., 2020).

The NXOR is located to the north of Jiangnan uplift, the east of Fanchang Basin and Tongling uplift, and the south of Ningwu volcanic basin (Fig. 1a, Wang et al., 2017; Yao et al., 2014, 2013; Li et al., 2009, 2008; Zheng et al., 2007, 2004; Wu et al., 2006; Zhao and Cawood, 1999). This region is mostly covered by Quaternary sediments, overlaying the continental clastic sedimentary and volcanic rocks since the Cretaceous. As well as the Liqiao anticlinorium, the fault system is in EW-NE direction, composed of the Qingshui-Hewan fault (QHF), Jiangnan fault (JNF), Zhouwang fault (ZWF), and Ningguo-Jixi fault (NJF). Intense Yanshanian magmatism within this region formed a series of intermediate-felsic volcanic and intrusive rocks.

Magmatism has strongly developed in this basin, forming a group of intermediate acid volcanic and intrusive rocks in the Jiulianshan, Jingtingshan, Huangniushan, and Chating areas. These volcanic rocks have a thickness of >100 m, and are characterized by pyroclastic rocks in the Lower Cretaceous. The intrusions, which are formed in the basement of the basin, are widely distributed and exposed in the Changshan-Shizishan-Kunshan-Tongshan-Magushan areas. Deep drilling data reveal that intrusions occur beneath the volcanic rocks, including pyroxene diorite, diorite, and porphyritic granodiorite (Fig. 1b; Xu et al., 2020; Lu et al., 2019).

Mineralization in the NXOR is strongly developed, forming variety of ore deposits, especially the large-scale Chating porphyry Cu-Au deposit, several medium-scale skarn Cu-W-Mo and hydrothermal Pb-Zn deposits. For the porphyry deposits, ore minerals occur in the porphyritic quartz diorites, and which outcrop in the tectonic fracture zones and contact zones of the intrusion for the skarn deposits. Mineralization has obvious accumulative characteristics, and been dominated by Cu-Au, Cu-Mo-(S), Cu-(S-W), Cu-Mo metallogenic in the centers, surrounded by Pb-Zn metallogenic, respectively (Fig. 1b). Recent geochronological and geochemical results (Qi et al., 2020, 2019; Xu et al., 2020; Lu et al., 2019; Qi, 2019; Zhou et al., 2019; Jiang et al., 2017, 2015) show that the major mineralization occurred in 145–135, 134–130, and 128–125 Ma. Besides the high-K calc-alkaline intermediate-felsic intrusions, the porphyry Cu-Au (i. e., Chating deposit) and skarn Cu-Mo-(S-W) deposits (i. e., Tongshan-Qiaomaishan and Magushan deposits) developed in the early stage. Hypabyssal intermediate acid intrusions and resulted skarn Cu-Mo deposits in the middle stage, while hydrothermal Pb-Zn polymetallic deposits developed in the late stage.

2 METHODS

2.1 Profile Array

We carried out high-resolution reflection seismic exploration on three major profiles (I, II, III) in the NXOR, with regional MT, gravity and magnet measurements. The results of multi-discipline geophysical profiles II and III are shown here for interpretation and discussion, because all the above geophysical exploration were carried out in these two profiles as well as the surface geological survey. Profile II has crossed the major geounits in the study area, including Tongling uplift, Nanling Basin,

Jingtingshan-Liqiao anticline, Xuancheng Basin, and Jiangnan orogenic belt. Profile III was divided into two sections (III-1 and III-2) owing to the presence of lakes, Nanling Basin, Jingtingshan-Liqiao anticline, Xuancheng Basin, the Jiangnan orogenic belt. Moreover, the Chating and Shizishan deposits are located on section III-1 (D02), while Magushan deposit is located on section III-2 (D01).

2.2 Data Acquisition and Processing

Seismic reflection profiling was performed using a 428XL seismograph (Sercel, France), MT soundings were obtained using a V5-2000 system (Phoenix, Canada), gravity measurements were recorded using a CG-5 gravimeter (Scintrex, Canada), and magnetic measurements were made using a GSM-19T proton magnetometer (GEM, Canada).

Seismic data for migration profiles were processed using a PROMAX seismic system. Stacking profiles were obtained by horizontal stacking after pretreatment, static correction, dynamic correction, stacking noise suppression, and deconvolution. The MT data were processed using the software of Prof. Shikun Dai from Central South University, Changsha, China, allowing a two-dimensional continuous media inversion for resistivity modeling. The corrections for observed gravity data included altitude correction, terrain correction and Bouguer correction, and the Bouguer gravity anomaly was then obtained. The magnetic anomaly was reduced to pole.

2.3 3D Geological Modeling

The 3D geological modeling was controlled by 2D parallel sections, using GeoModeller (Intrepid Geophysics, Australia). Profile models were obtained by a gravity, magnet, electric data processing software (RGIS2016) developed by China Geological Survey. The morphology and distribution of sedimentary strata and other rock units can be shown by the 3D modeling to understand the structure of the study area.

Regional 1 : 50 000 gravity and aeromagnetic data, seismic reflection results and 2D inversion models of MT data inversion have been used to establish the 3D geo-model. The average fit error of the 3D model is less than 10%, and the information error with the borehole and surface geological data is also less than 10%.

2.4 Effectiveness of the Prospecting Method

In the NXOR, geophysical data were acquired using effective detection methods for the deep structure. The specific physical property can be revealed by related geological methods, respectively. Different physical property has different response features in the geophysical results. For example, MT measurement reveals the spatial morphology of the structure through the difference of electrical properties, while gravity data reveal the density differences. To unify these physical properties reasonably, the 3D comprehensive geological model in this paper is the result of the full fit and understanding of gravity and magnetic anomalies, MT inversion models, and seismic reflections.

In addition, we have collected a large number of deep drillhole data. These data (e.g., ZK4102 at depth of 1 800 m in Chating ore region; Nanling 1 drilling at depth of 3 808.63 m and Wanxuan 1 drilling at depth of 2 750 m in the basin)

were used to verify and constrain our geological model in depth range of 0–5 km.

3 GEOPHYSICAL RESULTS AND INTERPRETATION

Results of the MT, gravity, and magnetic measurements for the three major profiles reveal the physical variations of the uppermost crust of our study region (Figs. 2, 3, 4), while the seismic reflections reveal the deep geological structure in a depth range of 0–15 km (Figs. 5, 6). The deep geological structures of our study area were constructed mainly based on seismic reflections and electrical models, considering about gravity and magnetic data and constraints of drillhole data. Four geo-units were identified and separated by the KITNS, JNF, and ZWF, forming a structure pattern composing of two anticlines and two basins (Figs. 1b, 7). The uplifted anticlinal areas exhibit a three-layer structure, and the basin areas show a two-layer structure. The specific geophysical comprehensive interpretations of deep geological structure are as follows.

3.1 Deep Structure of the Main Units

The two depression basins are named Xuancheng and Nanling basins, and the two folded uplifts are the Jingtingshan-Liqiao and Magushan-Yishan anticlinorium (Fig. 1b).

3.1.1 Nanling Basin

Nanling Basin is covered by the Quaternary sediments with some exposures of the Cretaceous and Paleogene rocks in the southwestern area (Figs. 1b, 7). It is a dustpan-shaped rifted basin, which is bounded by the QHF (directed in NE-SW) on the northwest and overlapped by a thrust-nappe system in the southeast. This basin is characterized by low gravity values (Fig. 2c) and two major electrical layers in the MT inversion models. At distance of 4.5–30.5 km of profile II, the shallow low-resistivity layer (0–1 800 m; $<30 \Omega \cdot \text{m}$) can be corresponded to the Cretaceous–Quaternary sediments, while the deeper high-resistivity layer (1 800–5 000 m; $>200 \Omega \cdot \text{m}$) can be attributed to the responses of Paleozoic–Triassic sediments (Fig. 2a). The thickness of shallow conductive layer varies in range of 1.8–2.5 km from the southwestern area to the northeast (Figs. 2a, 3a, 4a), indicating the variation of the lower boundary. The basement underlying the basin composes of the Ordovician–Triassic sediments, in which the Triassic unconformably overlies the Silurian rocks. However, the covers unconformably overlay on the Devonian rocks in the southwestern area.

3.1.2 Jingtingshan-Liqiao anticlinorium

The Jingtingshan-Liqiao anticlinorium locates in the center of the NXOR and separates the Nanling and Xuancheng basins. Silurian–Permian sediments are exposed on the surface with the Triassic rocks on both sides (Fig. 1b). This anticlinorium comprises the Xinhezhuang anticline, the Kunshan synclinorium, the Huashan syncline, and the Jingtingshan anticline. Moreover, it is indicated as a generally overturned anticline by the geophysical results. According to the D02 seismic reflection migration profile (Fig. 6), the strong reflection waves (Cambrian–Ordovician) suggests a compound anticline structure, with a center at CDP 3280. The southeastern limb of the Jingtingshan-Liqiao anticlinorium is well preserved, while

the northwestern limb has been strongly destroyed as a result of the thrusting of Liqiao fault (LQF). In the electrical model of profile III, a three-layer structure (Fig. 3a) is revealed with increasing resistivity from the surface to the deep. The conductive layer (0–200 m; $<50 \Omega \cdot \text{m}$) can be corresponded to the volcanic rocks, the middle transition zone (200–3 000 m; $50\text{--}300 \Omega \cdot \text{m}$) is suggested as the Paleozoic–Triassic sediments effected by the volcanism, and a deep resistive layer (3 000–5 000 m; $>300 \Omega \cdot \text{m}$) may indicate the deep batholith beneath Chating. Moreover, the vertically oriented resistivity body ($>300 \Omega \cdot \text{m}$) at distance of 21–23 km along the profile III can be inferred as the Chating ore-bearing intrusion, consistent with the ore-bearing porphyritic diorite revealed by the drillhole. Geological model of profile III-1 shows a large batholith under the Xinhezhuang anticline and Kunshan synclinorium (Fig. 3d), and the Paleozoic strata of Xinhezhuang anticline has thrusts on the Cretaceous volcanic rocks. However, the Xinhezhuang anticline is shown as a closed fold system instead of overturned structure in profile III-2 (Fig. 4d).

3.1.3 Xuancheng Basin

The Xuancheng Basin directed in NE-SW is covered by the Cretaceous–Quaternary sediments. It has been controlled by the KSF on its western margin, and developed into a dustpan shape, depressing towards the KSF during the sedimentation (Figs. 1b, 7). As shown in the seismic reflection migration profile D01 (Fig. 5), the reflection of the lower boundary (~ 2 km) of the Cretaceous strata (CDP 5660–4260, 1 s) is clear and shows a “bowl” shape with the center at CDP 4759. A series of arc-shaped reflections is revealed in the basement of this basin (below 1 s), and inferred as the Paleozoic–Triassic strata through the regional stratigraphic sequence. In the geo-electrical model of profile III-1 (along the profile, Fig. 3a), two major resistivity layers are at distance from 31 to 55 km. The lower resistive layer (50–200 $\Omega \cdot \text{m}$) composed of the Paleozoic–Triassic sediments underlies the Cretaceous volcanic rocks, causing conductive structure ($<20 \Omega \cdot \text{m}$). The center of the basin is located in Shencun with maximum thickness of ~ 2 km (Fig. 4a). For the eastern basin in profile III-2, a low-gravity anomaly with a width of ~ 8 km (Fig. 4c) is revealed. Angle unconformity is the major feature between the Paleozoic–Triassic and Cretaceous strata.

3.1.4 Magushan-Yishan anticlinorium

The Magushan-Yishan anticlinorium comprises two anticlines and is located in the eastern NXOR, exposing rarely (Figs. 1b, 7). Seismic reflection migration profile D01 (Fig. 5) shows a relatively clear reflection at CDP 2659–3559, corresponding to the lower boundary of Cretaceous strata (0.2 s). A series of wave-shaped reflections are revealed in double travel-time range of 0.2–2.0 s, attributing to the Paleozoic strata. The reflections beneath 2.0 s have scattered and indistinct characteristics, inferred as the responses of deep igneous rocks. The electrical profile III-2 (26–38 km) shows a resistive body ($>1 000 \Omega \cdot \text{m}$) (Fig. 4a), consistent with an E-W-oriented high-gravity anomaly (Fig. 4c). It can be inferred as the Paleozoic strata. The core of the anticline (profile 30–35 km) has exposed on the surface. A fault, which is indicated by a resistivity distortion zone at a depth of 1–2 km, is suggested separating the Silurian for-

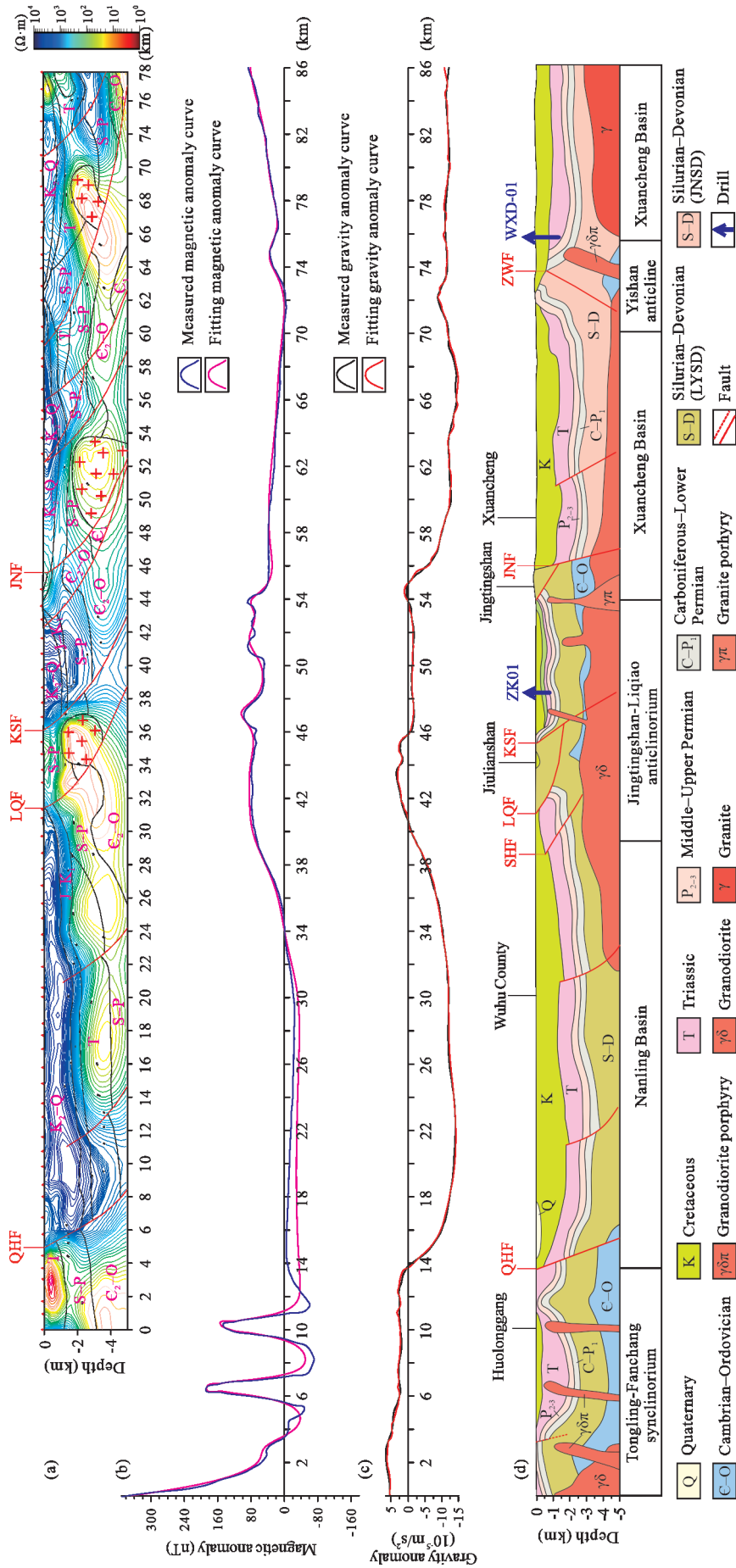


Figure 2. Resistivity structures from 2D MT inversion (a), magnetic anomaly curve (b), gravity anomaly curve (c), and the section of 3D-geological model (d) of the corridor II.

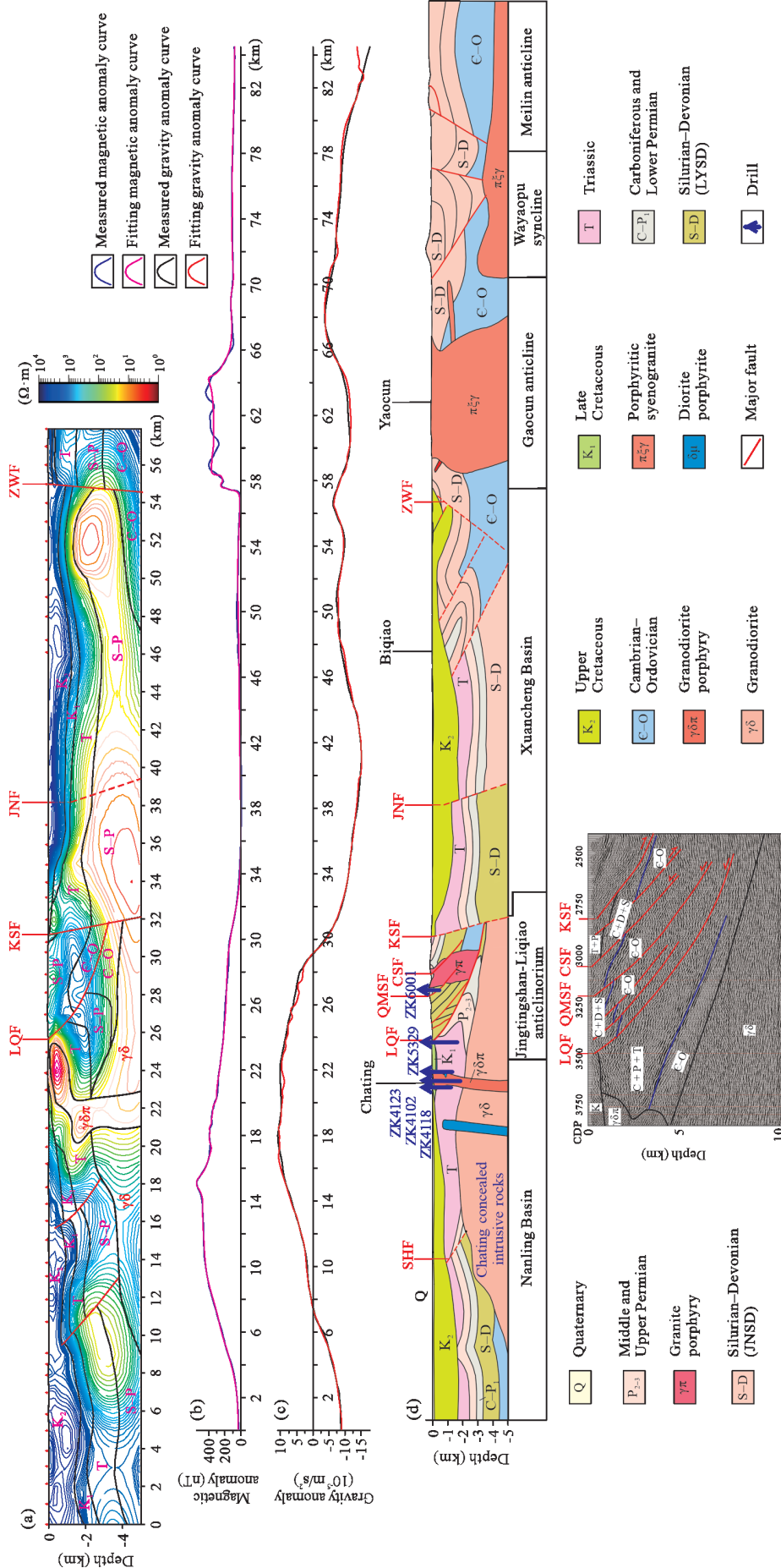
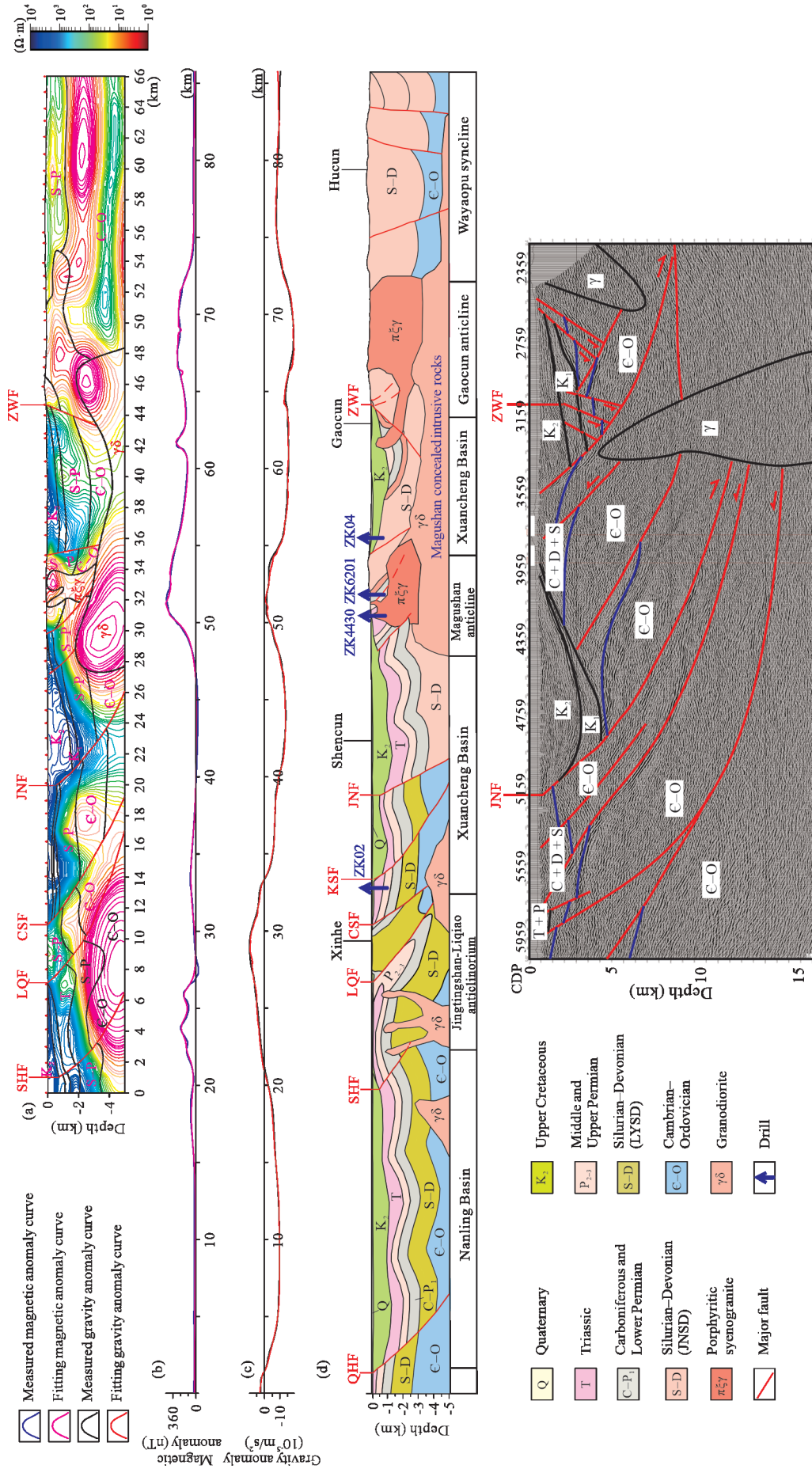


Figure 3. Resistivity structures from 2D MT inversion (a), magnetic anomaly curve (b), gravity anomaly curve (c), and the section of 3D-geological model (d) of the corridor III-1.



mation (profile ~30 km). Interpreted geological profile indicates a concealed and inverted Magushan anticlinorium, overlaying by the thick Cretaceous strata on profile III-1. Moreover, there are obvious Permian–Silurian units on profile III-1, forming an inverted syncline with Carboniferous strata in the anticlinal core (Fig. 3d). On profile III-2, an incomplete Magushan anticline is shown and can be attributed to the absent of southeastern limb because of the eroding. Its northwestern limb comprises Triassic–Silurian units. For the Yishan anticline, structures on profile II show a well developed northwestern limb comprising of Triassic–Silurian units, while a insidious southeastern limb controlled by faults (Fig. 2d). The structure of Magushan-Yishan anticlinorium is complicated and obscure due to the regional compression. As shown in Figs. 4d, 5, 6, there

may be a deep batholith in this area.

3.2 Major Faults

The fault system in the NXOR comprises “four longitudinal and two lateral” faults. The longitudinal faults in this ore district are QHF, KITNS, JNF, and SHF, while the lateral are ZNF and ZWF (Figs. 1b, 7). In addition, the QHF and ZWF have constrained the basin boundaries (Fig. 1b).

3.2.1 Qingshui-Hewan fault (QHF)

The QHF fault has controlled the development of Nanling Basin (Figs. 1b, 7). Lü et al. (2014) proposed that it was the main thrust-nappe structure in the MLYB and had controlled the formation of Tongling and Ningwu ore districts to the west.

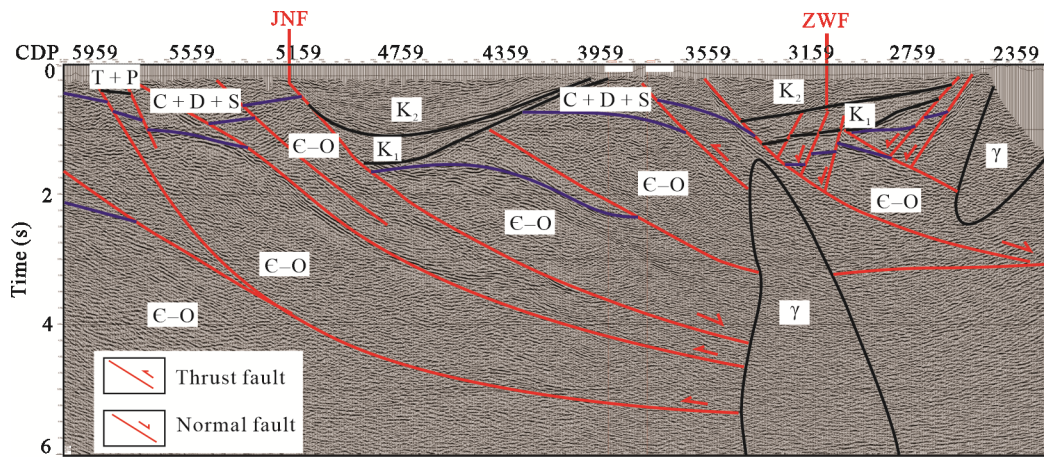


Figure 5. Migrated and interpreted reflection seismic section of line D01. C. Cambrian; O. Ordovician; S. Silurian; D. Devonian; C. Carboniferous; P. Permian; T. Triassic; K₁. Lower Cretaceous; K₂. Upper Cretaceous; γ . granites.

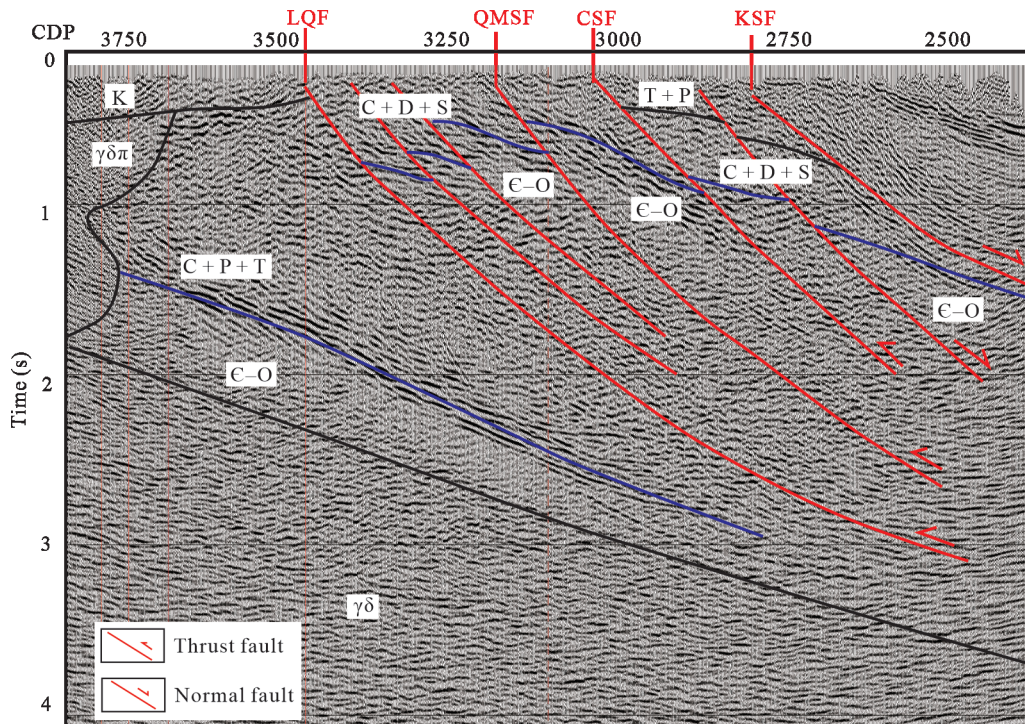


Figure 6. Migrated and interpreted reflection seismic of line D02. C. Cambrian; O. Ordovician; S. Silurian; D. Devonian; C. Carboniferous; P. Permian; T. Triassic; K. Cretaceous; $\gamma\delta\pi$. granodiorite porphyry; $\gamma\delta$. Granodiorite.

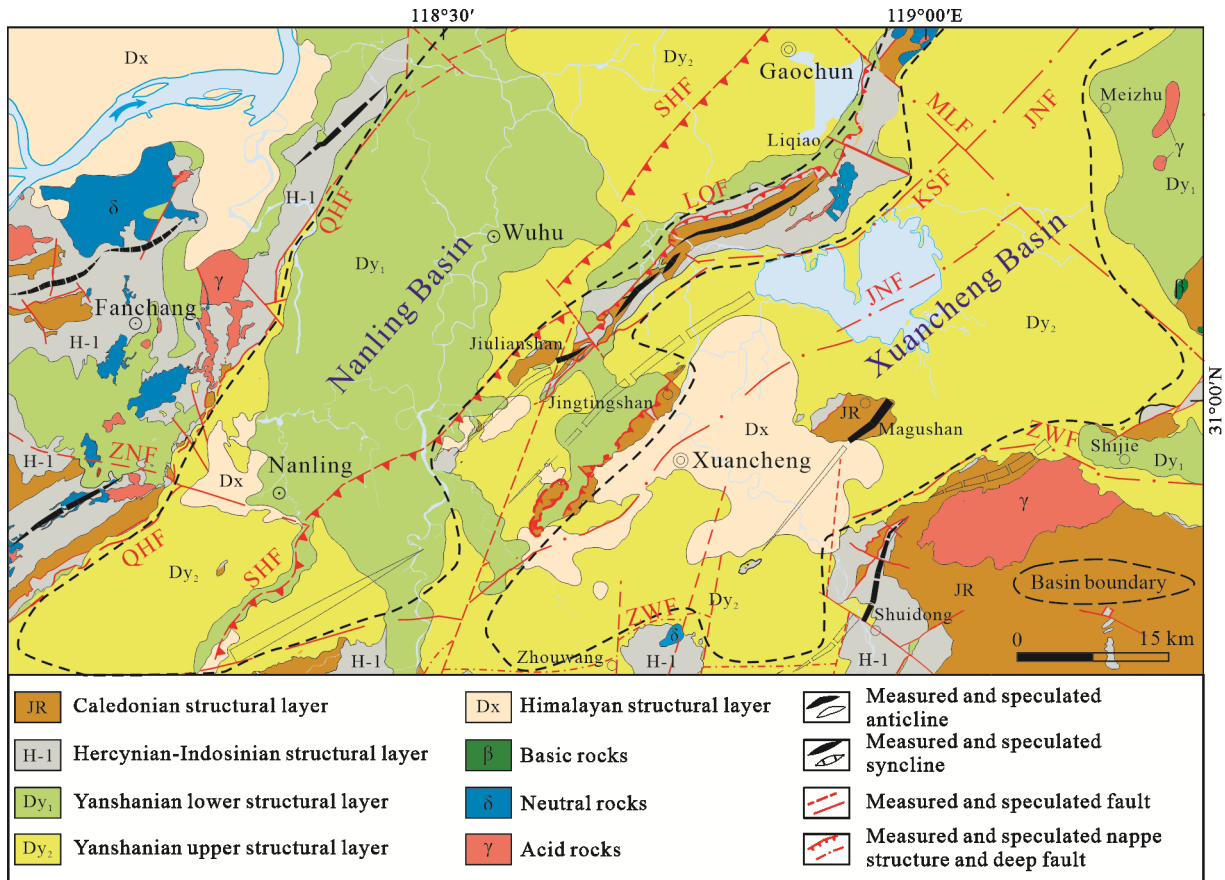


Figure 7. Structure outline map of the NXOR.

This normal fault is generally directed in NE-SW, dipping in 40° SE (Fig. 8a). High and low Bouguer gravity and magnetic anomalies are distributed on both sides of this fault, which is characterized by gradient zone. Furthermore, the structured variations are also revealed in the electrical model (Fig. 2a).

3.2.2 Sanlizhen-Hexizhen fault (SHF)

The SHF is a newly discovered concealed fault beneath the Nanling Basin (Figs. 1b, 7). This fault is evident by a gradient zone of gravity, magnetic, and electrical image (Figs. 2b, 2c). The SHF is a syn-orogen basement fault formed in the Indosinian, and does not cut the overlying Cretaceous strata. It is suggested as a thrust directed in NE-SW with gentle dipping.

3.2.3 Kunshan imbricate thrust-nappe structure (KITNS)

The shallow part of the KITNS consists retrograde anticline, NE directional thrust, and NW-trending strike-slip fault system, developing in the Paleozoic–Triassic strata (Figs. 1b, 9). Because a series of deposits in the NXOR occurred in the upper and lower plates of this thrust nappe, its geological structure is important for understanding the mineralization. According to the D02, the strong reflections at CDP 2850–3500 can be interpreted as the Cambrian–Ordovician strata (Fig. 6). The KITNS (0.5–2.5 s) with an 8 km extension is suggested as a thrust-nappe interface (LQF). A series of imbricate reflections identified in the upper plate represent the thrust-nappe schists, containing the sub-thrust faults at double travel-time of 0.3, 0.1, 0.1, and 0.25 s. These sub-thrusts may referred to the Qiao-

maishan fault (QMF), Chishan fault (CSF), and Kunshan fault (KSF) from the northeastern area to the southwest (Fig. 6). The major thrust interface is also revealed in electrical model of III-1 (Fig. 3a) between a resistivity and conductive layer at distance of 25 km, corresponding to the structure in the seismic profile. The KSF displayed as an abrupt transition in the electrical model (Fig. 3a) may have controlled the western boundary of the Xuancheng Basin.

3.2.4 Jiangnan fault (JNF)

The Jiangnan fault is not exposed on the most surface of the NXOR but appears in the Jingxian to the south of our study region (Fig. 8c). As an important target for our investigation, the JNF at CDP 5159–3559 dips steeply in the shallow area and separates the Cambrian–Ordovician and Precambrian strata (Fig. 5). Reflections on both sides of the JNF are significantly different, indicating the different basements of MLYB and Jiangnan Orogen. The Dongling basement is represented as a relatively conductive layer in the electrical model, on the northeast of JNF, while the Jiangnan basement on the southwest of JNF is resistive. The anomaly with high Bouguer gravity beneath the Jingtingshan-Liqiao area also represents the density differences between Dongling and Jiangnan basement, comparing with the Bouguer gravity data of Xuancheng area. The density of Dongling basement is higher than that of the Jiangnan basement.

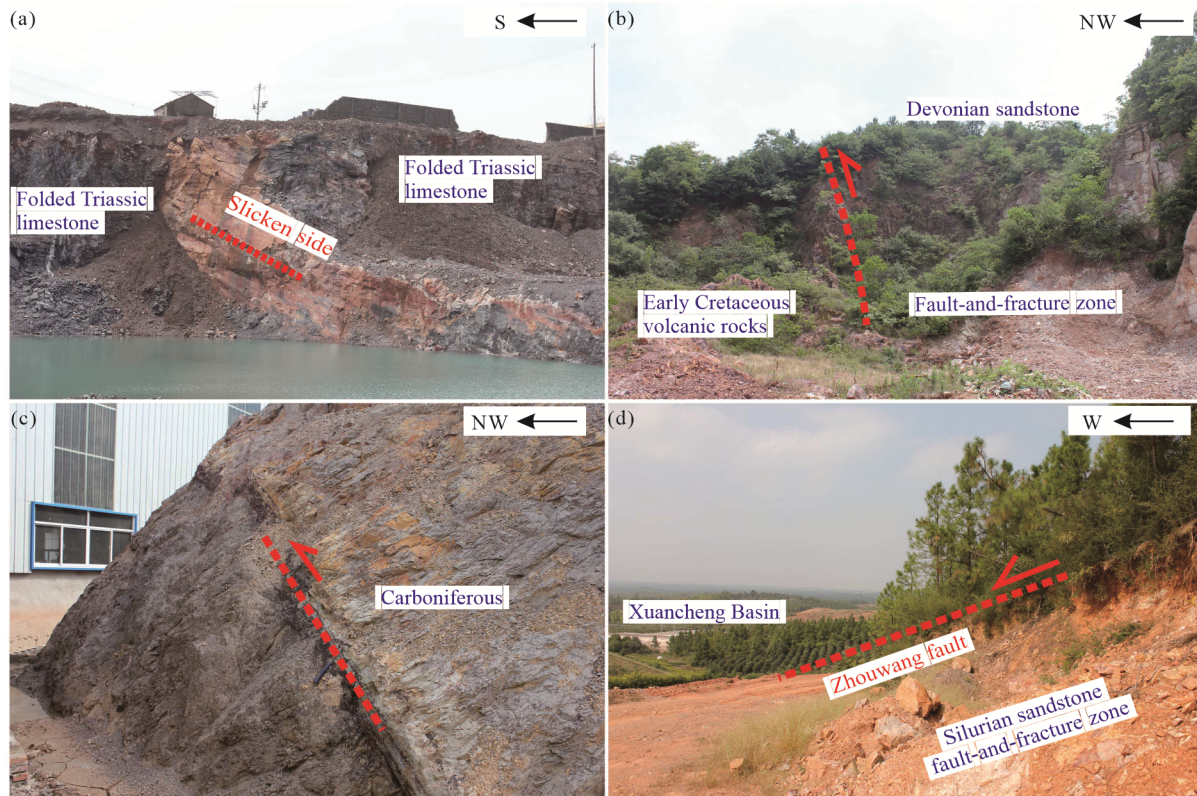


Figure 8. Field photographs showing the structural characteristics of major faults in the NXOR. (a) QHF, a sinistral strike-slip fault with normal component; (b) thrust fault exposed in the Yangxian area, the Devonian sandstone over the Early Cretaceous volcanic rocks; (c) JNF, a fault and wide fault-and-fracture zone developed in the Carboniferous; (d) ZWF, as a boundary normal fault, locates between the Silurian sandstone and the Xuancheng Basin.

3.2.5 Zhouwang fault (ZWF)

The ZWF is a boundary between the Lower Yangtze depression and the Jiangnan uplift (Figs. 1b, 7). This fault is generally directed in E-W and locally in ENE-WSW. The Paleozoic–Mesozoic strata with obvious fold structures formed on the south of the fault. The ZWF rarely exposed in our study region has formed into a thrust at first and transformed into a normal (Fig. 8d). According to the D01 (Fig. 5), a series of reflections dipping steeply to the northwest at DCP 3200–2800 cut through the arc-shaped reflections in range of 0–2 s. These structures are corresponding to a electrical gradient belt, and can be inferred to the ZWF (Fig. 5). Therefore, the ZWF are suggested as a series of normal faults, dipping in NW. In addition, Bouguer gravity anomalies also have obvious differences on sides of this fault.

3.2.6 Zhongming-Nanling fault (ZNF)

The ZNF is a concealed fault and may control the diagenesis. The fault directed in EW is located in the gravity gradient zone, showing obvious differences on both sides. On the aeromagnetic pole anomaly map, the fault exhibits a series of high magnetic anomalies on the background with high values. In the electrical model, this fault is represented as a isoline distortion zone.

3.3 Three-Dimensional Geological Model Interpretation

The 2D profiles can only reflect the features of geological bodies perpendicular to the tectonic strikes. To reveal the lateral

spatial morphology of the geological structures, the 3D model can better reflect the features of the geological bodies between the parallel profiles. In this study, the physical property parameters of the main geological bodies are collected and counted systematically (Table 1), and we constructed the 3D physical property units, including the Upper Cretaceous–Quaternary layer showing as a set of low resistivity and density layer; the Triassic layer exhibiting high-resistivity and high-density; the Silurian–Permian layer represented as the conductive and medium-density layer; the Upper Cambrian–Ordovician strata showing high resistivity and density instead of low resistivity and density in the Jiangnan area; the Lower Cambrian with low resistivity and medium-low density.

Figure 9a shows the 3D geological structure of the NXOR, and Fig. 9b shows the slices, revealing the 3D distribution of the major geological units in our study area. It is consistent with the geological profiles III-1 and III-2. In this model, the NXOR composes of two compound anticlines and two basins (Fig. 9a). The exposed area of the compound anticlines is 110 km², which occupies only 1.4% of the ore district. These anticlines compose of Silurian and Devonian strata that have been intruded by a large concealed batholith in the core (depth of 1.5 km). Constraining by the deep-drilling data, it is suggested superimposed by the KITNS overlying Paleozoic–Mesozoic strata forming a series of thrust faults extended to the Upper Cretaceous Chishan Formation or volcanic rocks (Fig. 9b). Some skarn deposits occurred in the contact zone between intrusions and limestone strata of the upper plate of this thrust

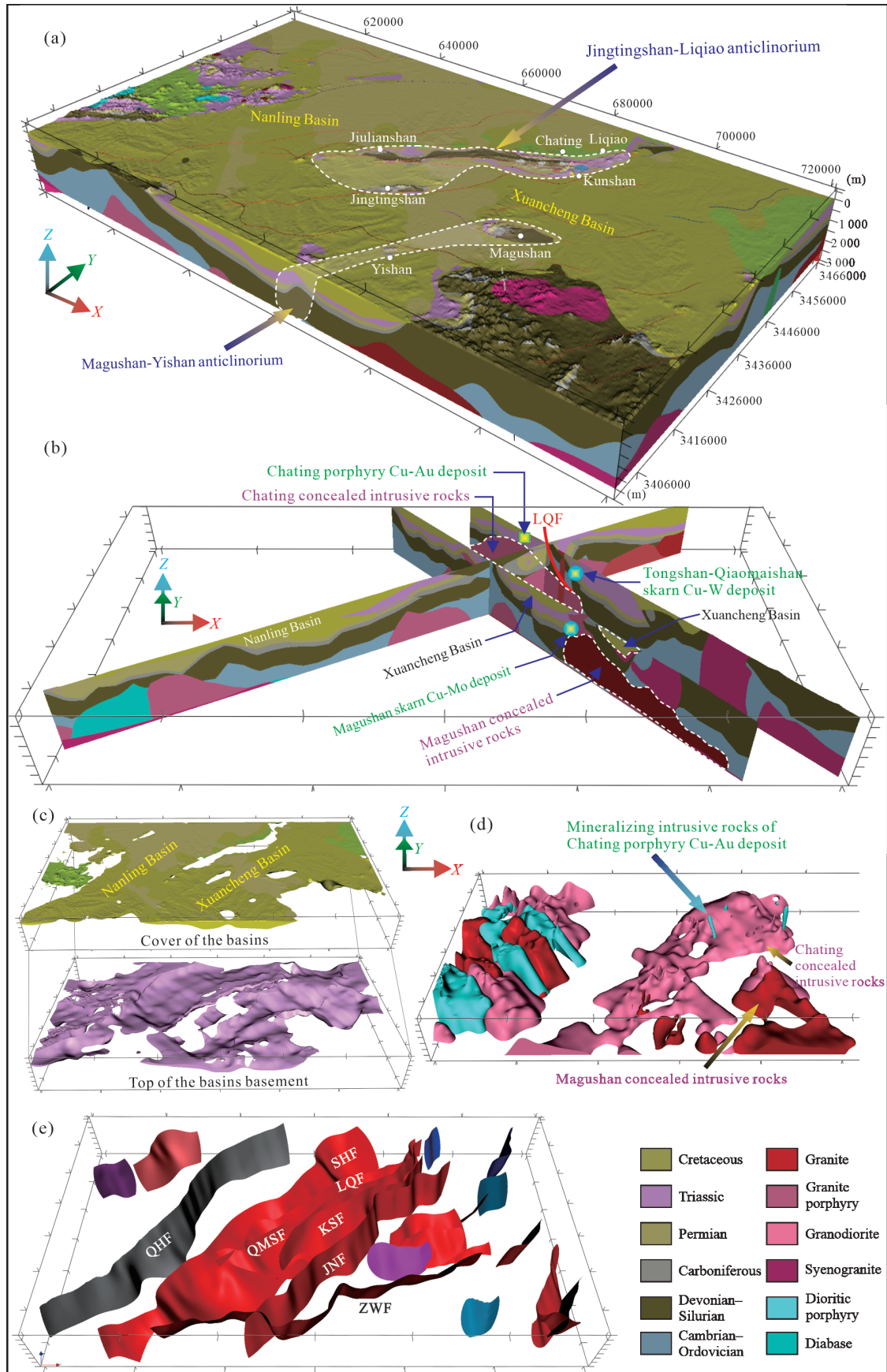


Figure 9. 3D-geological model of the NXOR. (a) 3D-geological model; (b) the sections of 3D-geological model including Chating Cu-Au deposit; LQF, basins and the concealed intrusive rocks; (c) 3D-geological model of the basins with “two layer structure”; (d) 3D-geological model of magmatic rocks; (e) 3D-geological model of faults.

Table 1 Physical parameters of modeling unit

Strata and rocks	Modeling unit code	Density (g/cm ³)	Magnetism ($\times 10^{-2}$ A/m)	Resistivity ($\Omega \cdot m$)
Quaternary	Q	1.87	0	0–10
Neogene–Upper Cretaceous	N–K ₂	2.36	0	500
Lower Cretaceous (Zhongfencun, Kedoushan, Dawangcun formations)	K _{1z} (K _{1d} , K _{1k})	2.40–2.44	20	800
Triassic	T	2.65–2.68	0	5 000–10 000
Middle and Upper Permian	P ₂₋₃	2.40	0	3 000
Carboniferous–Lower Permian	C–P _{1q}	2.69–2.7	0	15 000
Devonian–Silurian (Lower Yangtze region)	D–S _{1g}	2.52–2.56	0	10 000
Devonian–Silurian (Jiangnan region)	D–S _{1x}	2.5–2.52	0	10 000
Ordovician–Cambrian (Lower Yangtze region)	O–C	2.75	0	20 000
Ordovician–Cambrian (Jiangnan region)	O–C	2.65	0	20 000
Pyroxene diorite	$\gamma\delta$	2.65	120–150	5 000
Diabase	βE	2.63	150	20 000
Granodiorite (porphyry)	$\gamma\delta(\pi)$	2.60–2.69	120–150	50 000
Granite porphyry	$\gamma\pi$	2.50–2.54	80–100	50 000
Granodiorite batholith	$\gamma\delta$	2.65	250	20 000
Granosyenite (porphyroid)	$(\pi)\xi\gamma$	2.44	70–150	10 000
Quartz syenite porphyry	$\pi\delta o$	2.57–2.62	146	5 000
Diorite (porphyrite)	$\delta(\mu)$	2.58	80–120	6 000
Orthophyre	$\xi\pi$	2.42	0–50	8 000
Monzonitic granite	$\eta\gamma$	2.6	200–230	2 000
Coarse porphyrite	$\tau\alpha\pi$	2.55	0	2 000
Quartz (diorite) monzonite	$\eta(\delta)o$	2.57–2.62	150–200	2 000
Quartz diorite (porphyry)	$(\pi)\delta o$	2.57–2.62	150–210	3 000

structure, such as the Tongshan-Qiaomaishan Cu-S-(W) deposit. However, porphyry deposits related to the deep concealed pluton have formed in the porphyritic quartz diorite in the Cretaceous Chishan Formation or volcanic rocks of the lower plate, such as the Chating Cu-Au deposit (Fig. 9b). The three-layer structure of the Magushan-Yishan anticline is clearly revealed (Fig. 9b). The shallow part (<1 000 m) is an inverted anticline, and the core has been intruded by an intrusion. The southeastern limb composes of Paleozoic strata, and the northwestern limb was inverted. The deep part (>1 000 m) composes primarily of a deep concealed intrusion and its differentiated smaller branches. The Magushan skarn deposit occurs in the contact zone between this intrusion and Paleozoic strata. Drilling data show that the two limbs of the Yishan anticline comprise Chishan Formation at depths <1 500 m, while fold structure in the Paleozoic–Mesozoic strata are appeared at depths >1 500 m.

In the other hand, the basins have a two-layer structure (Fig. 9c), clearly presenting in the reflection seismic and MT results. Nanling Basin is thick in the northwestern part and thin in the southeast, in which (Fig. 9c) the bottom boundary of the basin (Upper Triassic) ranges from 1.0 to 2.5 km in depth. In the south and east of this basin, the thickness decreases in the transition zone beneath the Jinglingshan-Liqiao complex anti-

cline. The basement of the basin is a large buried intrusion comprising granodiorite (Fig. 9d), which is related to the concealed deep faults (Fig. 9e). Compared with the Nanling Basin, the Xuancheng Basin is smaller and shallower in central parts because of folding and uplift. Therefore, there are several sub-uplifts and sub-depressions in this region. In our study region, the basements of both Nanling and Xuancheng basins are Triassic and older sedimentary strata, which tectonic pattern is a series of anticlines and synclines.

4 DISCUSSION

4.1 Mineralizational Constraints of the Deep Plutons

Based on the above results and interpretations, the deep and concealed Chating and Magushan plutons are suggested to be the “source region” of the mineralization in the NXOR.

The Chating porphyritic granodiorite pluton is located beneath the eastern Nanling Basin and the Xinhezhuang anticline. The shallower part (<6 km) has a maximum width of 20 km and has been cut by the KSF in the southeast (Fig. 3d). It is located at CDP 3858–3750 of seismic profile D02 (Fig. 6), showing weak and disorder reflections. The aeromagnetic anomaly indicates that this pluton has a shallowest top depth of 0.86 km between the northern Shuiyang and southern Gaochun, while the

depth increases in western Chating at ~1.3–1.5 km. Local high magnetic anomalies with different orientations may be attributed to localized shallow intrusion and mineralization. These porphyritic granodiorite intrusions may control the mineralization of Cu-Au deposit, example for the Chating deposit. The intrusion beneath Chating is covered by the Middle Cretaceous volcanics with a top depth of 100 m. In the electrical model, it is represented by a resistor, in which the conductive body can be corresponds to the Chating Cu-Au deposit (Fig. 3a).

The Magushan pluton is located beneath Magushan-Dawang area. The shallower part (<6 km) has a maximum width of 8 km, and a maximum width of 1 km on the top (Fig. 4d). The seismic reflections has absent in this pluton (Fig. 5). The top depth of this intrusion is ~2.8 km (1.4 s). A fault above this intrusion may be the channel for mineral migration. Aeromagnetic results suggest Magushan pluton is directed in N-S with a extension decreasing to the deep. It suggests that the upper part of the pluton is granodiorite with high magnet and density, and the lower part is porphyritic granodiorite with high magnet and low density. Its distribution is consistent with the responses in the electrical model (Fig. 4a).

The intrusive-related metal deposits have occurred in the shallower part of the Chating and Magushan plutons. Chating porphyry Cu-Au deposit can be attributed to the shallow part of the Chating concealed pluton. Together with the peripheral Tangjiazui hydrothermal-vein Pb-Zn deposits, a Chating-Tangjiazui mineralization area can be defined. The skarn-type Cu-Mo deposit can be attributed to the granodiorite in the shallower part of the Magushan pluton. Together with several hydrothermal-vein Pb-Zn polymetallic deposits, the Magushan mineralization area can be defined. These two areas are characterized by a high-temperature mineralization in the center and low-temperature mineralization all around. Although the deposit characteristics of location, time and mineralization are different in these two areas, hydrothermal fluids and associated minerals are suggested coming from the deep concealed intrusions. Therefore, the future porphyry-type and skarn-type deposit prospecting can focus on the contacted zones between the shallower intrusions differentiated from the deep and the carbonate strata.

4.2 Mineralization Constraints of the Deep Tectonics

The KITNS and JNF are suggested the channels for the magmatic-hydrothermal migration and providing spaces for mineralization in the NXOR.

4.2.1 Constraints of the KITNS

The KITNS is the southern extension of the Maoshan nappe structure and exposed in the Liqiao-Juilianshan area (Fig. 7). In this study, detailed field investigation results show that the KITNS directed in NE-SW across the Nanling Basin, the Jingtingshan-Liqiao anticlinorium, and the Xuancheng Basin. It can be separated into the Liqiao-Xinhe and Xinhe-Juilianshan sections (Fig. 1b). Nappe structures have been superimposed on the Liqiao anticlinorium, and characterized by the overturned anticline, significant NE directed thrust, and NW strike-slip fault system (Fig. 8b). The NE directed thrust is cut by NW directed strike-slip fault, forming a complex fault structural system. A series of imbricated faults are shown in the

reflected seismic profile. These imbricated faults are exposed on the surface, and compose of the Liqiao, Qiaomaishan, Chishan, and Kunshan thrust faults from northern area to the south. The Liqiao and Kunshan faults are the northern and southern boundary of this fault system, presenting extensional features in the early development stage. Therefore, these imbricate faults may control the metallogenesis.

The Chating porphyry Cu-Au deposit is found in the lower plate of KITNS, and the drilling data indicate the KITNS has not affected the ore body (Fig. 10). However, the skarn and magmatic-hydrothermal deposits (Tongshan-Qiaomaishan, Changshan, Shuangjing, and Shizishan) found in the upper plate of KITNS have been controlled by the limb, faults, and interlayer fractures of the inverted anticline. The ore-bodies occurred in the contact zones between clastic rocks and carbonate rocks, fracture zones between carbonate rocks and intrusions, and the contact zones between intrusions and surrounding rocks (Fig. 10). Therefore, the Early Cretaceous mineralization was controlled by the multi-stage activities of this nappe structure. During the Early Cretaceous, the KITNS has reactivated, and controlled the mineralization with the fold and interlayer slips. It is obvious that this thrust nappe makes it potential to search for the distal skarn-type or magmatic-hydrothermal type deposits in the lower plate.

4.2.2 Constraints of the JNF

The JNF spanned the South China is a large-scale and deep fault controlling the deformation since the Mesoproterozoic (Yang, 1988, 1981). Previous studies have focused on the western section of this fault, while the eastern section in Anhui Province gained less attention because of the large-scaled sediment cover (Fig. 7). The JNF is a concealed fault in the NXOR (Fig. 8c) and is directed mostly NE-SW. It is an important boundary between the Lower Yangtze basin and the Jiangnan uplift, originating from subduction-collision process between the Cathaysia and Yangtze blocks and controlling the back-arc basin in the Yangtze (Zheng et al., 2020). Moreover, This fault was reactivated during the Caledonian and Hercynian orogenies and formed the present pattern during the Indosinian intra-continental orogeny. The Xikou Group developed in the back-arc basin on southeast of this fault instead of the northwestern area, causing the Kongling-Dongling and Jiangnan basements on both sides of the JNF (Fig. 10). The Kongling-Dongling basement rocks on north of the JNF have a high density and low resistivity, while Jiangnan basement rocks have low density and low resistivity.

On north of the JNF, the intrusions compose mainly of porphyritic quartz diorite and characterized by high-K calc-alkaline. These intrusions are enriched in large-ion lithophile elements (LILEs; e.g., K, Rb, Sr, and Ba) and light rare-earth elements (LREEs), and is depleted in high-field-strength elements (HFSEs; e.g., Nb, Ta, and Ti) (Qi et al., 2020; Xu et al., 2020). It also shows weak Eu anomalies, but high ratios of Sr/Y and La/Yb, indicating adakitic feature. The plutons are also enriched in whole-rock Sr-Nd isotope compositions ($(^{87}\text{Sr}/^{86}\text{Sr})_i = 0.706\text{--}0.707$, $\epsilon_{\text{Nd}}(t) = -6.9$ to -9.1 ; Qi et al., 2020; Jiang et al., 2017), the Hf isotope composition of zircon ($\epsilon_{\text{Hf}}(t) = -6.7$ to -12.2), old two-stage model age ($T_{\text{DM2}} = 1.5\text{--}2.0$ Ga), and the

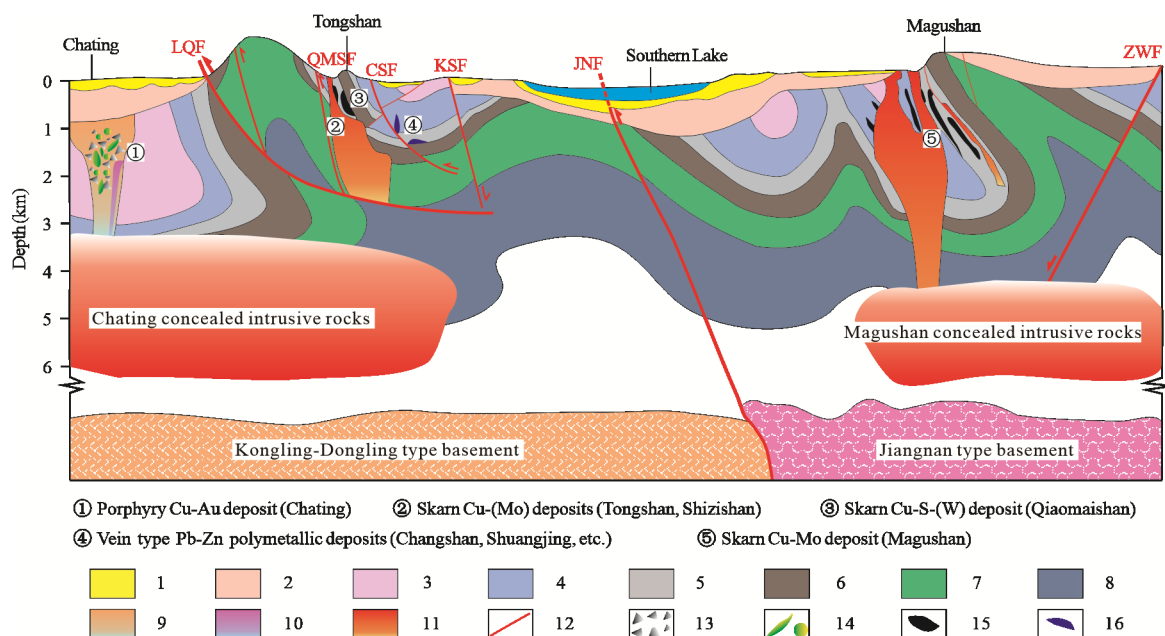


Figure 10. The relationship between shallow geological structure and mineralization in the NXOR to a depth of 5 km. 1. Quaternary; 2. Cretaceous; 3. Triassic; 4. Permian; 5. Carboniferous; 6. Devonian; 7. Silurian; 8. Cambrian–Ordovician; 9. quartz diorite porphyrite; 10. dioritic porphyrite; 11. granodiorite; 12. faults; 13. crytoexplosive breccia; 14. veined and disseminated copper-gold ore bodies; 15. copper-molybdenum bodies; 16. copper-tungsten bodies.

Paleoproterozoic inherited zircons (Qi et al., 2020). These results suggest that the primitive magma derived from the basalt of enriched lithospheric mantle and mixed with ancient Yangtze Block crustal material (Xu et al., 2019; Jiang et al., 2017). The porphyry Cu-Au and skarn Cu-Mo-W-S deposits occurred in these intrusions have been timing in 139 Ma (Xu et al., 2019) and 133 Ma (Lu et al., 2020), coherent with the ore bearing magmatic rocks (quartz diorite porphyrite and granodiorite porphyry). Moreover, and the metal minerals and ore-forming hydrothermal fluids are related to magmatic-hydrothermal fluids (Lu et al., 2020; Qi et al., 2020; Xiao et al., 2019, 2018; Xu et al., 2018). The above diagenesis and mineralization can be attributed to the products of the first stage (146–135 Ma) of the MLYB (Lu et al., 2020).

In the other hand, the magmatic activity of first stage on south of the JNF can be represented by the Magushan pluton, showing different geochemical characteristics with the Chating pluton. The Magushan granodiorites are I-type granites characterized by peraluminous and high alkalinity (Qi et al., 2019). These intrusions are enriched in LILEs and depleted in HFSEs (Qi et al., 2019). Comparing with the porphyrites, these granodiorites have higher $(^{87}\text{Sr}/^{86}\text{Sr})_i$ (0.708–0.710) and $\epsilon_{\text{Nd}}(t)$ (-5.4 to -5.2) values, as well as higher zircon $\epsilon_{\text{Hf}}(t)$ values of -4.6 to -1.4 and younger two-stage model ages ($T_{\text{DM2}} = 1.5\text{--}1.2$ Ga; Qi et al., 2019). These characteristics suggest that the magma source of these intrusive rocks originated from enriched lithospheric mantle, mixing the Neoproterozoic crustal materials of the Jiangnan uplift. It is consistent with the metallogenic rocks of the W-Mo-Cu deposits in the eastern Jiangnan uplift (150–135 Ma; Gu et al., 2017; Yan et al., 2017; Song et al., 2014; Xue et al., 2009). These geochemical differences also indicate that the variation of basement materials has played a key role in mineralization of the NXOR (Chang et al., 2019; Zhou et al., 2017). The Magushan skarn Cu-Mo deposit, which was

associated with the Magushan pluton, developed on the south of JNF and formed in 143.8 Ma (Lu et al., 2020), coherent with the formation age of metallogenic host rock (136.4–135.3 Ma; Xu et al., 2020; Qi et al., 2019). The aforementioned mineralization event can be classify into the first mineralization stage (150–135 Ma) in the eastern Jiangnan uplift, relating to skarn-type W-Mo-Cu deposit (Lu et al., 2020; Qi et al., 2019).

5 CONCLUSION

Combining high-resolution geophysical measurements and previous drilling data, we constructed 3D geological model of the NXOR in a depth range of 0–5 000 m and obtained new insights as follows.

(1) The ore region shows a structural pattern including two anticlines and two basins, and contains a “four longitudinal and two lateral” fault system. The basins exhibit a two-layer structure, comprising basement consisting of Triassic strata overlain by Cretaceous to Quaternary rocks.

(2) Major structures associated with mineralization are JNF and KITNS. The JNF controls both lithofacies and crustal basements, causing different mineralization types.

(3) Two deep concealed plutons associated with the formation of the Chating porphyry-type Cu-Au deposit has been found by our measurements, which oriented from the differentiation and emplacement of the intermediate-acid diorite.

ACKNOWLEDGMENTS

This article was supported by the National Key R&D Program Project of China (No. 2016YFC0600209). We are grateful to the project principal of Qingtian Lü for his excellent organization and leadership, Academician Yinbo Chang for his long-term support and guidance on the project, and Prof. Chuanzhong Song for his guidance, and deserve thanks to Shilong Qian, Zujun Xie, and Qianguo Yang from the No. 322 Geologi-

cal Unit of Bureau of Geology and Mineral Exploration of Anhui Province, No. 812 Geological Unit of East-China Metallurgical Bureau of Geology and Exploration for their helps and assistances. The final publication is available at Springer via <https://doi.org/10.1007/s12583-021-1577-x>.

REFERENCES CITED

- Chang, Y. F., Li, J. H., Song, C. Z., 2019. The Regional Tectonic Framework and some New Understandings of the Middle-Lower Yangtze River Valley Metallogenic Belt. *Acta Petrologica Sinica*, 35(12): 3579–3591 (in Chinese with English Abstract)
- Chang, Y. F., Liu, X. P., Wu, Y. C., 1991. The Copper-Iron Belt of the Lower and Middle Reaches of the Changjiang River. Geological Publishing House, Beijing, 1–379 (in Chinese)
- Dong, S. W., Ma, L. C., Liu, G., et al., 2011. On Dynamics of the Metallogenic Belt of Middle-Lower Reaches of Yangtze River, Eastern China. *Acta Geologica Sinica*, 85(5): 612–625 (in Chinese with English Abstract)
- Feng, T. L., Liu, J., Li, K., et al., 2018. Geological Characteristics and Genesis of Shizishan Copper (Molybdenum) Deposit in Xuancheng City, Anhui Province. *Modern Mining*, 37(7): 21–26 (in Chinese with English Abstract)
- Gu, H. L., Yang, X. Y., Deng, J. H., et al., 2017. Geochemical and Zircon U-Pb Geochronological Study of the Yangshan A-Type Granite: Insights into the Geological Evolution in South Anhui, Eastern Jiangnan Orogen. *Lithos*, 284/285: 156–170 <https://doi.org/10.1016/j.lithos.2017.04.007>
- Guo, D., Yan, J. Y., Lü, Q. T., et al., 2014. 3D Density Mapping Constrained by Geological Information: Model Study and Application. *Acta Geologica Sinica*, 88(4): 763–776 (in Chinese with English Abstract)
- Hong, D. J., Huang, Z. Z., Chan, S. W., et al., 2017. Geological Characteristics and Exploration Directions of the Cu-Polymetallic Ore Deposits in the Magushan-Qiaomaishan Areas in Xuancheng, Anhui Province. *East China Geology*, 38(1): 28–36 (in Chinese with English Abstract)
- Heinson, G., Didana, Y., Soeffky, P., et al., 2018. The Crustal Geophysical Signature of a World-Class Magmatic Mineral System. *Scientific Report*, 8(1): 10608. <https://doi.org/10.1038/s41598-018-29016-2>
- Ji, K., 2018. Mineralogy and Fluid Inclusion Geochemistry of the Chating Cu-Au Deposit, Xuancheng City, Anhui Province: [Dissertation]. Hefei University of Technology, Hefei. 1–79 (in Chinese with English Abstract)
- Jiang, F., Xu, X. C., Qian, S. L., et al., 2017. Zircon U-Pb Age and Genesis of the Ore-Bearing Quartz-Dioritic Porphyries in the Chating Cu-Au Ore Deposit, Xuancheng City, Anhui Province. *Geological Journal of China Universities*, 23(4): 591–605 (in Chinese with English Abstract)
- Jiang, F., Xu, X. C., Wang, M., et al., 2015. Characteristics and Geochronometry of Magmatic Rocks in the Chating Cu-Au Ore District, Xuancheng City, Anhui Province. *Acta Geologica Sinica*, 89(Suppl.): 144–147 (in Chinese with English Abstract)
- Lan, X. Y., Du, J. G., Yan, J. Y., et al., 2015. 3D Gravity and Magnetic Interactive Inversion Modeling Based on Prior Information: A Case Study of the Tongling Ore Concentration Area. *Chinese Journal of Geophysics*, 58(12): 4436–4449 (in Chinese with English Abstract)
- Li, X. H., Li, W. X., Li, Z. X., et al., 2008. Ma Bimodal Volcanic and Intrusive Rocks in Northern Zhejiang, South China: A Major Episode of Continental Rift Magmatism during the Breakup of Rodinia. *Lithos*, 102(1/2): 341–357. <https://doi.org/10.1016/j.lithos.2007.04.007>
- Li, X. H., Li, W. X., Li, Z. X., et al., 2009. Amalgamation between the Yangtze and Cathaysia Blocks in South China: Constraints from SHRIMP U-Pb Zircon Ages, Geochemistry and Nd-Hf Isotopes of the Shuangxiwu Volcanic Rocks. *Precambrian Research*, 174(1/2): 117–128. <https://doi.org/10.1016/j.precamres.2009.07.004>
- Liu, X. M., 2016. Ore Characteristics of the Tongshan-Qiaomaishan Cu-S Deposit in Xuancheng City, Anhui Province. *Modern Mining*, 32(4): 127–130 (in Chinese with English Abstract)
- Liu, X. M., Duan, L. A., 2015. Geological Features and Metallogenic Regularity of the Tongshan-Qiaomaishan Cu-S-W-Fe Polymetallic Ore Deposit in Xuancheng City. *Geology of Anhui*, 25(3): 174–178 (in Chinese with English Abstract)
- Lü, Q. T., Liu, Z. D., Tang, J. T., et al., 2014. Upper Crustal Structure and Deformation of Lu-Zong Ore District: Constraints from Integrated Geophysical Dats. *Acta Geologica Sinica*, 88(4): 447–465 (in Chinese with English Abstract)
- Lü, Q. T., Liu, Z. D., Yan, J. Y., et al., 2015. Crustal-Scale Structure and Deformation of Lu-Zong Ore District: Joint Interpretation from Integrated Geophysical Data. *Interpretation*, 3(2): SL39–SL61. <https://doi.org/10.1190/int-2014-0211.1>
- Lü, Q. T., Meng, G. X., Zhang, K., et al., 2021. The Lithospheric Architecture of the Lower Yangtze Metallogenic Belt, East China: Insights into an Extensive Fe-Cu Mineral System. *Ore Geology Reviews*, 132: 103989. <https://doi.org/10.1016/j.oregeorev.2021.103989>
- Lü, Q. T., Meng, G. X., Yan, J. Y., et al., 2020. The Geophysical Exploration of Mesozoic Iron-Copper Mineral System in the Middle and Lower Reaches of the Yangtze River Metallogenic Belt: A Synthesis. *Earth Science Frontiers*, 27(2): 232–253 (in Chinese with English Abstract)
- Lü, Q. T., Tang, J. T., Liu, Z. D., 2012. Crustal Structure of Tongling Ore District and its Control on Mineral Genesis, as Revealed by Inergrated Geophysical Profiles. Abstract in 34th IGC, August 5–10, Brisbane
- Lü, Q. T., Yan, J. Y., Shi, D. N., et al., 2013. Reflection Seismic Imaging of the Lujiang-Zongyang Volcanic Basin, Yangtze Metallogenic Belt: An Insight into the Crustal Structure and Geodynamics of an Ore District. *Tectonophysics*, 606: 60–77. <https://doi.org/10.1016/j.tecto.2013.04.006>
- Lu, S. M., Yang, Q. G., Qi, H. S., et al., 2019. A Geological-Geophysical Model for the Chating Copper-Gold Deposit, Xuancheng, Anhui Province. *Acta Geologica Sinica—English Edition*, 93(Suppl. 1): 243–244. <https://doi.org/10.1111/1755-6724.14061>
- Lu, S. M., Zhang, Z. Z., Zhao, L. L., et al., 2020. Genetic Types, Spatio-temporal Distribution of Ore Deposits and Sources of Ore-Forming Materials in the Xuancheng Area, Anhui Province. *Acta Geologica Sinica—English Edition*, 94(6): 1874–1892. <https://doi.org/10.1111/1755-6724.14605>
- Mao, J. W., Xie, G. Q., Duan, C., et al., 2011. A Tectono-Genetic Model for Porphyry-Skarn-Stratabound Cu-Au-Mo-Fe and Magnetite-Apatite Deposits along the Middle-Lower Yangtze River Valley, Eastern China. *Ore Geology Reviews*, 43(1): 294–314. <https://doi.org/10.1016/j.oregeorev.2011.07.010>
- Qi, G., Lü, Q. T., Yan, J. Y., et al., 2014. 3D Geological Modeling of Luzong Ore District Based on Priori Information Constrained. *Acta Geologica Sinica*, 88(4): 466–477 (in Chinese with English Abstract)
- Qi, H. S., Lu, S. M., Yang, X. Y., et al., 2020. The Role of Magma Mixing in Generating Granodioritic Intrusions Related to Cu-W Mineralization: A Case Study from Qiaomaishan Deposit, Eastern China. *Minerals*, 10(2): 171. <https://doi.org/10.3390/min10020171>
- Qi, H. S., Lu, S. M., Yang, X. Y., et al., 2019. Formation of the Granodiorite-Hosting Magushan Cu-Mo Polymetallic Deposit in Southern Anhui,

- Eastern China: Evidences from Geochronology and Geochemistry. *Minerals*, 9(8): 475. <https://doi.org/10.3390/min9080475>
- Qi, H. S., 2019. Comparing Geochemical Study of Porphyry Copper-Gold Deposits in Different Tectonic Environments: A Case Study of Grasberg, Papua, Indonesia and Chating, Anhui Province: [Dissertation]. University of Science and Technology of China, Hefei. 1–143 (in Chinese with English Abstract)
- Qian, S. L., Yang, Q. G., Xie, Z. J., et al., 2017. Geological Features and a Discussion of Ore-Forming Conditions of the Chating Porphyry Copper(Gold) Ore Deposit in the Xuancheng District, Anhui Province. *Geology of Anhui*, 27(2): 81–86 (in Chinese with English Abstract)
- Song, G. X., Qin, K. Z., Li, G. M., et al., 2014. Mesozoic Magmatism and Metallogeny in the Chizhou Area, Middle-Lower Yangtze Valley, SE China: Constrained by Petrochemistry, Geochemistry and Geochronology. *Journal of Asian Earth Sciences*, 91: 137–153. <https://doi.org/10.1016/j.jseae.2014.04.025>
- Tang, J. T., Zhou, C., Ren, Z. Y., et al., 2014. Three Dimensional Magnetotelluric Inversion and Structural Framework of Tongling Ore District, Anhui. *Acta Geologica Sinica*, 88(4): 598–611 (in Chinese with English Abstract)
- Tang, J. T., Zhou, C., Wang, X. Y., et al., 2013. Deep Electrical Structure and Geological Significance of Tongling Ore District. *Tectonophysics*, 606: 78–96. <https://doi.org/10.1016/j.tecto.2013.05.039>
- Wang, M., 2018. A Study on the Geological and Geochemical Characteristics and Genesis of the Chating Cu-Au Ore Deposit in Xuancheng City, Anhui Province: [Dissertation]. Hefei University of Technology, Hefei. 1–66 (in Chinese with English Abstract)
- Wang, X. L., Zhou, J. C., Chen, X., et al., 2017. Formation and Evolution of the Jiangnan Orogen. *Bulletin of Mineralogy, Petrology and Geochemistry*, 36(5): 714–735, 696 (in Chinese with English Abstract)
- Wu, R. X., Zheng, Y. F., Wu, Y. B., et al., 2006. Reworking of Juvenile Crust: Element and Isotope Evidence from Neoproterozoic Granodiorite in South China. *Precambrian Research*, 146(3/4): 179–212. <https://doi.org/10.1016/j.precamres.2006.01.012>
- Xiao, Q. L., Zhou, T. F., Wang, S. W., et al., 2019. Genesis of Chating Cu-Au Deposit in the Middle-Lower Yangtze River Metallogenic Belt, Eastern China: Implications from Magnetite and Biotite Geochemistry. *Ore Geology Reviews*, 106: 113–133. <https://doi.org/10.1016/j.oregeorev.2019.01.017>
- Xiao, Q. L., Zhou, T. F., Yuan, F., et al., 2018. Compositional Characteristics, Petrogenesis and Metallogenic Significance of Biotite from the Ore-Bearing Quartz Diorite Porphyry in Chating Cu-Au Deposit, Anhui Province. *Mineral Deposits*, 37(6): 1179–1194 (in Chinese with English Abstract)
- Xiao, X., Tang, J. T., Zhou, C., et al., 2011. Magnetotelluric Sounding in the Lujiang-Zongyang Ore District and Preliminary Study of Electrical Structure. *Acta Geologica Sinica*, 85(5): 873–886 (in Chinese with English Abstract)
- Xiao, X., Wang, X. Y., Tang, J. T., et al., 2014. Conductivity Structure of the Lujiang-Zongyang Ore Concentrated Area, Anhui Province: Constraints from Magnetotelluric Data. *Acta Geologica Sinica*, 88(4): 478–495 (in Chinese with English Abstract)
- Xie, Z. J., Zhang, L., Zhou, X. F., 2018. Geological Characteristics and Comprehensive Indexes of the Porphyry Copper-Gold Deposit in Chating, Anhui Province. *Modern Mining*, 8: 53–55 (in Chinese with English Abstract)
- Xu, X. C., An, Y. H., Xu, X. Y., et al., 2020. Zircon U-Pb Ages and Element Geochemistry Characteristics of Magmatic Rocks in Nanling-Xuancheng Area of Anhui, China. *Journal of Earth and Environment*, 42(1): 15–35 (in Chinese with English Abstract)
- Xu, X. C., Ji, K., Bai, R. Y., et al., 2018. Modes of Occurrence of Gold and Genetic Connection between Gold and Copper in the Ores from the Chating Porphyry Copper-Gold Deposit, Xuancheng City, Anhui Province. *Acta Petrologica et Mineralogica*, 37(4): 575–589 (in Chinese with English Abstract)
- Xu, X. C., Xu, X. Y., Xie, Q. Q., et al., 2019. Geological and Geochemical Characteristics and Genesis of the Chating Copper-Gold Deposit in Xuancheng City, Anhui Province. *Acta Petrologica Sinica*, 35(12): 3659–3676 (in Chinese with English Abstract)
- Xue, H. M., Wang, Y. G., Ma, F., et al., 2009. Zircon U-Pb SHRIMP Ages of the Taiping (Calc-Alkaline)-Huangshan (Alkaline) Composite Intrusion: Constraints on Mesozoic Lithospheric Thinning of the Southeastern Yangtze Craton, China. *Science in China Series D: Earth Sciences*, 52(11): 1756–1770. <https://doi.org/10.1007/s11430-009-0133-9>
- Yan, J., Hou, T. J., Wang, A. G., et al., 2017. Petrogenetic Contrastive Studies on the Mesozoic Early Stage Ore-Bearing and Late Stage Ore-Barren Granites from the Southern Anhui Province. *Science in China Series D: Earth Sciences*, 47(11): 1269–1291 (in Chinese)
- Yan, J. Y., Lü, Q. T., Chen, X. B., et al., 2014. 3D Lithologic Mapping Test Based on 3D Inversion of Gravity and Magnetic Data: A Case Study in Lu-Zong Ore Concentration District, Anhui Province. *Acta Petrologica Sinica*, 30(4): 1041–1053 (in Chinese with English Abstract)
- Yan, J. Y., Lü, Q. T., Meng, G. X., et al., 2009. Aeromagnetic 3D Inversion Imaging for Intermediate-Acid Intrusive Bodies and its Indication for Deep Ore Prospecting in Tongling Ore Concentration District. *Mineral Deposits*, 28(6): 838–849 (in Chinese with English Abstract)
- Yan, J. Y., Lü, Q. T., Zhao, J. H., 2019. Local Uplift and Copper Metallogenic Prospect in the Luzong Ore District, Eastern China: Evidence from 3D Magnetotelluric Imaging. *Exploration Geophysics*, 50(1): 22–30. <https://doi.org/10.1080/08123985.2018.1563454>
- Yang, Z. J., 1981. On the Nature of a Zone of Abrupt Stratigraphic, Rockfacies and Paleontological Changes in the Jiangnan Region. *Geological Review*, 27(2): 123–129 (in Chinese with English Abstract)
- Yang, Z. J., 1988. Study on the Jiangnan Middle-Macro seismic Belt. *Seismology and Geology*, 10(2): 14–18 (in Chinese with English Abstract)
- Yao, J. L., Shu, L. S., Santosh, M., et al., 2013. Geochronology and Hf Isotope of Detrital Zircons from Precambrian Sequences in the Eastern Jiangnan Orogen: Constraining the Assembly of Yangtze and Cathaysia Blocks in South China. *Journal of Asian Earth Sciences*, 74: 225–243. <https://doi.org/10.1016/j.jseae.2012.08.010>
- Yao, J. L., Shu, L. S., Santosh, M., et al., 2014. Palaeozoic Metamorphism of the Neoproterozoic Basement in NE Cathaysia: Zircon U-Pb Ages, Hf Isotope and Whole-Rock Geochemistry from the Chencai Group. *Journal of the Geological Society*, 171(2): 281–297. <https://doi.org/10.1144/jgs2013-036>
- Zhang, K., Lü, Q. T., Yan, J. Y., 2015. The Lower Crust Conductor from Nanjing (Ning)-Wuhu (Wu) Area in the Middle and Lower Reaches of Yangtze River: Preliminary Results from 3D Inversion of Magnetotelluric Data. *Journal of Asian Earth Sciences*, 101: 20–29. <https://doi.org/10.1016/j.jseae.2015.01.007>
- Zhang, K., Lü, Q. T., Yan, J. Y., et al., 2019. The Subduction and Continental Collision of the North China and Yangtze Blocks: Magnetotelluric Evidence from the Susong-Anqing Section of Western Anhui, China. *Geophysical Journal International*, 216(3): 2114–2128. <https://doi.org/10.1093/gji/ggy541>

- Zhao, G. C., Cawood, P. A., 1999. Tectonothermal Evolution of the Mayuan Assemblage in the Cathaysia Block: Implications for Neoproterozoic Collision-Related Assembly of the South China Craton. *American Journal of Science*, 299(4): 309 – 339. <https://doi.org/10.2475/ajs.299.4.309>
- Zheng, H. W., Li, T. D., He, R. Z., 2020. Southeastward Subduction of North China Block: Insights from Tomographic Image of the Middle and Lower Yang-tze River Metallogenic Belt. *Earth Science*, 45(11): 4187–4197. <https://doi.org/10.3799/dqkx.2020.053> (in Chinese with English Abstract)
- Zheng, Y. F., Wu, Y. B., Chen, F. K., et al., 2004. Zircon U-Pb and Oxygen Isotope Evidence for a Large-Scale ^{18}O Depletion Event in Igneous Rocks during the Neoproterozoic. *Geochimica et Cosmochimica Acta*, 68(20): 4145–4165. <https://doi.org/10.1016/j.gca.2004.01.007>
- Zheng, Y. F., Zhang, S. B., Zhao, Z. F., et al., 2007. Contrasting Zircon Hf and O Isotopes in the Two Episodes of Neoproterozoic Granitoids in South China: Implications for Growth and Reworking of Continental Crust. *Lithos*, 96(1/2): 127–150. <https://doi.org/10.1016/j.lithos.2006.10.003>
- Zhou, T. F., Fan, Y., Yuan, F., et al., 2008. The Geochronology of the Volcanic Rocks in Luzong (Lujiang-Zongyang) Basin and Its Significance, Anhui Province. *Science China: Earth Sciences*, 38(11): 1342–1353 (in Chinese)
- Zhou, T. F., Fan, Y., Wang, S. W., et al., 2017. Metallogenic Regularity and Metallogenic Model of the Middle-Lower Yangtze River Valley Metallogenic Belt. *Acta Petrologica Sinica*, 33(11): 3353 – 3372 (in Chinese with English Abstract)
- Zhou, T. F., Wang, S. W., Yuan, F., et al., 2016. Magmatism and Related Mineralization of the Intracontinental Porphyry Deposits in the Middle-Lower Yangtze River Valley Metallogenic Belt. *Acta Petrologica Sinica*, 32(2): 271–288 (in Chinese with English Abstract)
- Zhou, Y. Z., Zhao, L. L., Jin, M., et al., 2019. Diagenetic Chronology of Mashanbu Pluton in Xuancheng Area, Anhui Province and Its Geological Significance. *Geology of Anhui*, 29(2): 81–85 (in Chinese with English Abstract)